Design and Control of an Axial-Flux Machine for a Wide Flux-Weakening Operation Region

Tae-Suk Kwon, *Member, IEEE*, Seung-Ki Sul, *Fellow, IEEE*, Luigi Alberti, *Student Member, IEEE*, and Nicola Bianchi, *Member, IEEE*

Abstract—This paper describes the strategy to design and control an axial-flux (AxF) surface-mounted permanent-magnet machine for achieving a wide flux-weakening (FW) operating region. By using a slotted stator with fractional-slot windings and additional cores enclosing end windings, the AxF machine satisfies the specification of a wide constant-power speed range. The design procedure is presented for increasing FW capability while obtaining low-harmonic back electromotive force and low cogging torque. This technique is applied to design an 8-N · m AxF prototype machine that exhibits about 3 : 1 FW range. To the aim of exploiting full capability of the machine, an FW controller is designed and implemented. This controller utilizes the voltage difference between the current regulator and the output voltage, limited by a voltage source inverter. With this method, the output torque in the FW region is higher than that achieved using the conventional FW method based on the voltage-magnitude feedback. The goodness of both design and control algorithm is proved by experimental tests on a prototype.

Index Terms—AC motor drives, axial-flux (AxF) motor, flux-weakening (FW) control, fractional-slot machines.

I. INTRODUCTION

THE axial-flux (AxF) permanent-magnet machine has been focused on in several applications such as gearless elevator systems, wind power generation systems, and traction systems for hybrid or electric vehicles [1]–[3]. This machine topology has many attractive characteristics such as high efficiency and superior torque density. Moreover, due to its inherently short axial length, it is suitable for the electric traction machine as in-wheel direct-drive motor. In the last decade, many configurations of AxF machine have been proposed, including machines with slotted winding, slotless winding, and coreless winding [1]–[5]. For an in-wheel drive vehicle, the motor has to exhibit a flux-weakening (FW) operating region,

i.e., a constant-power speed range (CPSR), over 3 : 1. The coreless-type machine and the slotless-type machine exhibit low inductance because of their large effective air-gap length. In a slotted stator machine, a higher CPSR is achieved, besides it is not always enough. Therefore, the machine and power electronics have to be oversized so as to match the torque and speed specifications.

Several design approaches to increase the CPSR of the AxF machine can be adopted. External inductances can be added to the winding, besides increasing weight and cost. A proper slot opening of semiclosed slot might be designed, even though this is difficult to be realized by adopting the AxF lamination. A deep slot could be an alternative, avoiding decreasing the mechanical strength of the structure. Magnetic wedges can be inset to close the open slots of the stator. In [6], a magnetic wedge made by soft magnetic material is used to close the slot, reaching the FW range almost equal to 2 : 1. In [5], the mechanical device which adjusts the relative angle between two rotors according to the machine speed is used to reduce the back electromotive force (EMF) during high-speed operations. This method is not suitable for hard environment like a vehicle due to the lack of reliability of the mechanical device. In [7], an additional winding to weaken the magnet flux is introduced, but this additional winding decreases the power density as well as the machine efficiency. Other methods have been tried [8], [9], but they have too complex rotor or stator structures yielding to a very expensive solution.

From the viewpoint of the machine control, the AxF machine is basically equivalent to the radial-flux surface-mounted permanent-magnet (SPM) machine. There are many researches on the topic of the FW control of the SPM motors [10]–[13]. Among them, the algorithms presented in [13] show acceptable dynamic performance and superior static performance. The maximum output torque in the FW region is comparable to that of the six-step operation while maintaining the current-control capability.

This paper deals with the design of an AxF machine with slotted stator. Fractional-slot winding and additional cores enclosing end windings are adopted for increasing the inductance and then the FW capability. The proposed solution is also characterized by a low-back-EMF harmonic content and a low cogging torque.

In addition, this paper describes an FW controller designed to exploit full capability of the AxF machine drive. The described techniques are applied to design and to control an 8-N · m AxF machine prototype that exhibits about 3 : 1 FW range. The goodness of both design and control algorithm is proved by the experimental tests on the prototype.

TABLE I
STATOR GEOMETRY DATA

Outer Diameter	D_e	150 mm
Inner Diameter	D_i	80 mm
Difference between radii	h_r	35 mm
Slot height (available)	h_s	21 (16) mm
Slot width	w_s	12 mm
Back iron height	h_{bi}	24 mm
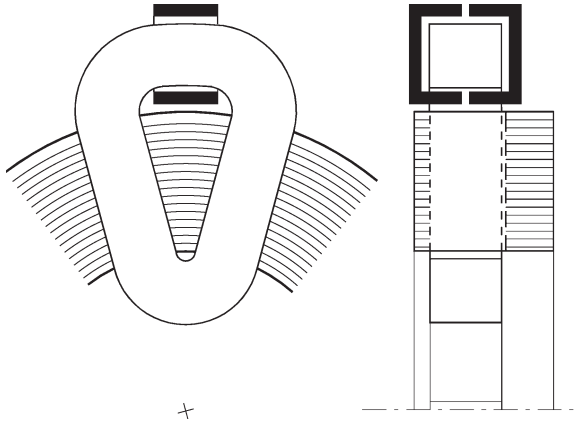
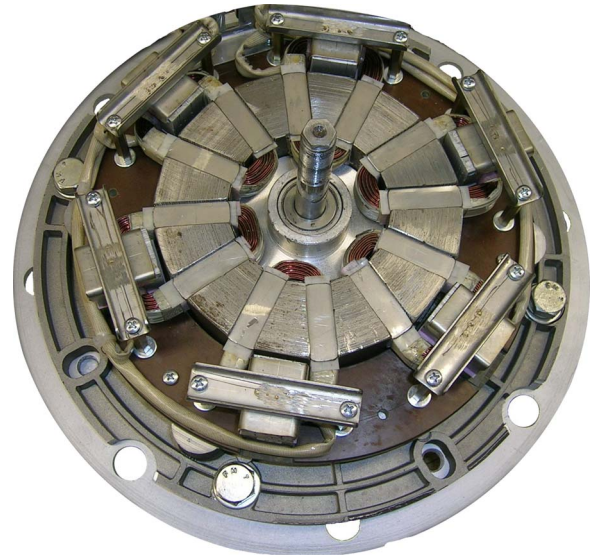Fig. 1.   Sketch of the stator geometry of the prototype.

Fig. 2.   Stator with six coils. The double cores in the end winding and their support are visible. The supports are removable in order to test the prototype without cores.

TABLE II
ROTOR GEOMETRY DATA

Brass separator width	w_{sp}	8 mm
Residual flux density	B_{rem}	1.1 T
Relative differential permeability	μ_{rec}	1.05
Air gap	g	1 mm
PM thickness	t_m	4 mm
PM cover angle	$2\alpha_m$	140 el deg

II. MACHINE-DESIGN PROCEDURE

This section deals with the design of an AxF machine able to exhibit a CPSR equal to three. As described in the Introduction, for achieving a wide speed range with an SPM machine, a large value of the inductance is necessary. For this purpose, a slotted commercial stator lamination has been selected. The main geometrical data of the stator are reported in Table I.

Laminated C-shape double cores are introduced into each end winding, as shown in Fig. 1 (solid line). With this configuration, the flux path remains in the lamination direction while the additional flux follows separate paths. Since the C-shape cores are laminated, the additional iron losses, due to the additional leakage flux, are limited. Of course, the use of such C-shape cores increases the outer diameter of the machine. In the built prototype, using commercial cores, the increase of external diameter is about equal to 40 mm. However, by optimizing the core figures and placing them over the lateral part of the coils, instead of the external radial part, the increase of the outer diameter can be estimated equal to 20 mm.

There is a remarkable advantage in using such cores in the external part of the motor. They allow an easy adjustment of the synchronous inductance of the machine. Thus, the same motor can be adopted for various applications, requiring or not a wide CPSR. The inductance is changed by bringing near or dividing the two parts of the external coils.

A further solution to increase the inductance that has been considered in this paper is to use magnetic wedges in the slot openings. Some tests on the AxF machine prototype with these magnetic wedges are reported in Section IV.

In order to increase the inductance, it is possible to take advantage of the winding configuration. A fractional-slot winding has been selected that typically exhibits an inductance higher than the corresponding integer slot winding [14]. In [15], a fractional-slot winding is used for increasing the CPSR

capability of a 42-slot 14-pole radial-flux SPM motor. In the AxF prototype, a 12-slot 10-pole motor configuration has been chosen. This slot/pole combination is characterized by a high magnetizing inductance, owing to the high magnetic energy in the air gap. In [14], it has been demonstrated that the inductance of a double-layer winding is almost 1.8 times higher than that of a motor with the same geometry and number of pole but distributed winding and one slot per pole per phase.

Always to the aim of increasing the inductance, a single-layer winding should be preferred. In this case, the inductance is double, becoming almost 3.6 times higher than that of a motor with distributed winding and one slot per pole per phase. A further advantage in using a single-layer winding is the slight increase of the average torque with respect to the double layer, owing to the higher distribution factor, from 0.966 to unity [14]. However, such winding arrangement has not only advantages. The fractional-slot single-layer winding yields high-magnetomotive-force space-harmonic contents that cause rotor losses, even though the total magnetic thickness (given by the sum of air-gap and permanent-magnet (PM) thickness) is high.

In conclusion, the winding is characterized by six coils, wound around a single tooth, so that each coil side is contained in one slot, as shown in Figs. 1 and 2. The slot throw results in $y_q = 1$ in number of slots. The rotor is formed by an iron disk on which the PMs are fixed by brass separators. In order to avoid any PM radial movement, a raised border has been manufactured in the disk. The main rotor data, including the PMs' characteristics, are reported in Table II. In Fig. 3, a rotor picture is shown, pointing out both PMs and brass separators.
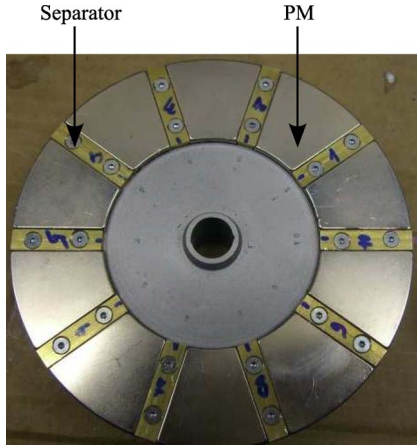
Fig. 3. The ten-pole AxF machine rotor. PMs and brass separators are recognizable.

Let us remember that the increase of the synchronous inductance in the SPM motor is necessary to widen the CPSR. Anyhow, such an increase yields a decrease of the power factor of the machine. For a given output power, this implies a higher volt–ampere rating of the converter. This has to be considered in the design of the electrical drive.

A. Motor Design

For a given CPSR requirement, it is possible to estimate the proper machine parameters, as reported in [16]. In particular, the normalized values of the flux linkage, inductance, and rated current are computed on the basis of the following specifications: the required CPSR, the base speed, the base power, the nominal voltage, and the machine saliency ratio $\xi = l_q/l_d$ (equal to one in an SPM machine). For the considered machine: CPSR $= 3$, $n_b = 1000$ r/min, $P_b = 1$ kW, and $V_b = 165$ V are fixed.

Fixing the normalized parameters quantity $v_n = 1$, $t_b = 1$, $\omega_b = 1$ per unit, the normalized PM flux linkage is computed on the basis of the required CPSR. Imposing a power $p_{fw} = 1$ per unit at the speed $\omega_{fw} = 3$ per unit (i.e., $CPSR = 3$), the normalized PM flux linkage results in $\lambda_m = 0.8$ per unit. Thus, as reported in [17], the normalized inductance and current are given by

$$l_d = l_q = \lambda_m \sqrt{1 - \lambda_m^2} \qquad (1)$$

$$i = \frac{1}{\lambda_m} = 1.25 \text{ per unit.} \qquad (2)$$

The second step of the motor design is to get the actual motor parameters corresponding to their normalized values. Hereinafter, the machine design is described, considering only one conductor per slot. The drawback of the completely open slot is a very high Carter's coefficient. On the other hand, an open slot allows the obtaining of a very high fill factor. It is $k_{\text{fill}} = 0.6$ in the prototype, considering the available slot surface $S_{\text{slot}} = 12 \times 16 = 192$ mm^2. The average value of the air-gap flux density is

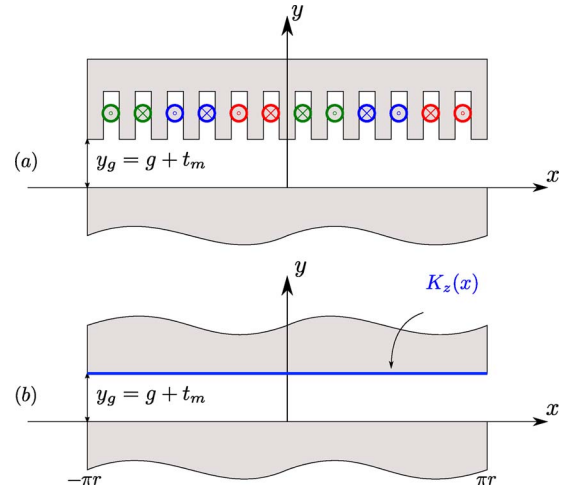$$B_{g0} = \frac{B_{\text{rem}}}{1 + \mu_{\text{rec}} \frac{k_C \, g}{t_m}} = 0.81 \text{ T} \qquad (3)$$

where k_C is the Carter factor (the average value for various radii). Other symbols are defined in Table II.

The peak value of the fundamental wave of the air-gap flux density is

$$\hat{B}_{g1} = \frac{4}{\pi} B_{g0} \sin(\alpha_m) = 0.95 \text{ T} \qquad (4)$$

where $\sin(\alpha_m)$ is the average value for various radii. By integrating the elementary flux of the fundamental harmonic from inner to outer radius, the fundamental flux per pole results in $\Phi_1 = 0.78$ mWb. According to the chosen winding arrangement, the flux linkage with one conductor per slot is

$$\Lambda_1 = k_w \frac{4n_c}{2} \left(\frac{2}{\pi} \hat{B}_{g1} \right) S_p = 1.47 \text{ mV} \cdot \text{s} \qquad (5)$$

where k_w is the winding factor and $S_p = (\pi/4)(D_e^2 - D_i^2)/2p$ is the pole surface. The bearings are selected on the basis of the axial force between stator and rotor that is estimated as $F = 3300$ N. The rated current density is fixed at $J = 4.5$ A/mm^2, on the basis of thermal considerations. The copper area is $S_{\text{Cu,slot}} = S_{\text{slot}} k_{\text{fill}} = 115.2$ mm^2. The peak current is $\hat{I}_{\text{slot}} = 730$ A. The rated torque results in $T = (3/2)p\Lambda_1 \hat{I}_{\text{slot}} = 8$ N $\cdot$ m. The torque can also be estimated considering the interaction between the flux density due the PM and the electric load. The latter is expressed by integrating the force density over the air-gap surface, obtaining the same value earlier.

A particular care is given in the design of the motor inductance. The latter is a key motor parameter when a wide CPSR is required; therefore, a proper value is essential to satisfy the requirements.

1) Slot Leakage Inductance: The slot leakage inductance is computed by classical equation [18]. It results in $L_{\sigma,\text{slot}} = 0.151$ μH, always considering one conductor per slot.

2) Air-Gap Inductance: The air-gap inductance is computed by solving the Maxwell equations in a 2-D space, since it has been verified that a simpler model is not accurate enough. A straight-lined 2-D cross section at the dummy radius r of the machine is considered, as shown in Fig. 4(a). The slotted configuration is transformed by removing the slots, as shown in

Fig. 4. Simplified model for the air-gap inductance computation, where g and t_m are given in Table II and r is the dummy radius.
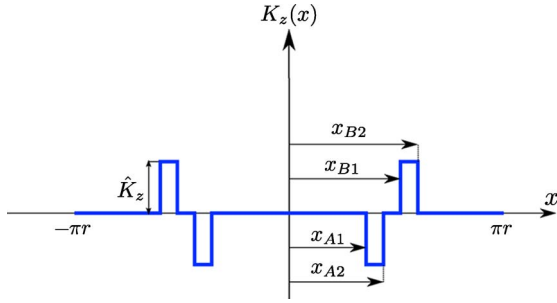
Fig. 5. Considered current density distribution in the thin sheet placed on the stator surface.
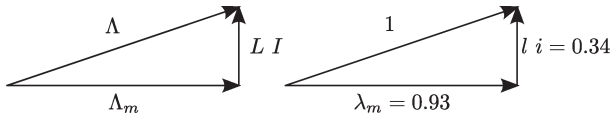
Fig. 6. Phasor diagram at rated operating point.

Fig. 7. Geometry of the additional core in the end winding (measurements in millimeters).
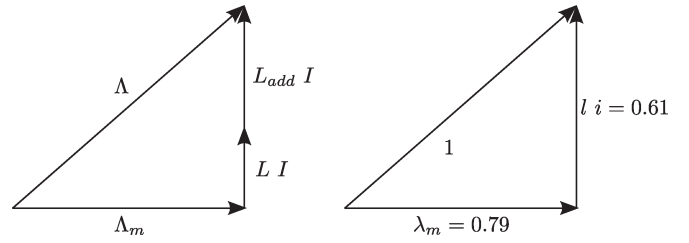
Fig. 8. Phasor diagram of the machine with the additional inductance.
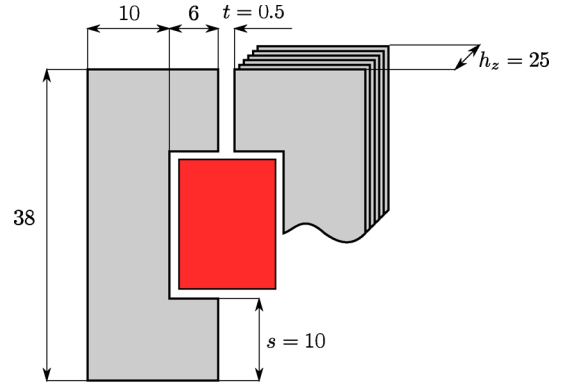
Fig. 4(b). The actual distribution of the conductors is replaced by an infinitesimal thin sheet placed on the stator surface. The waveform of the linear current density distribution $K_z(x)$ is shown in Fig. 5 and can be easily expressed by means of Fourier series expansion.

Solving the 2-D field problem in the air gap, the vector potential results in

$$A_z(x,y) = \sum_{n=1}^{\infty} \frac{a_n \mu_0 r}{n} \cdot \frac{\cosh \frac{ny}{r}}{\sinh \frac{ny_g}{r}} \cdot \cos \frac{nx}{r} \qquad (6)$$

where r is the considered radius of the straight-lined cross section and the series coefficients are expressed as

$$a_n = \frac{4\hat{J}_z}{n\pi} \sin \frac{nw_s}{2r} \left\{ \cos \frac{nx_B}{r} - \cos \frac{nx_A}{r} \right\} \qquad (7)$$

where w_s is the slot width, i.e., $w_s = x_{A2} - x_{A1} = x_{B2} - x_{B1}$, and $x_A = (x_{A1} + x_{A2})/2$, $x_B = (x_{B1} + x_{B2})/2$. From the field solution, the total energy is computed by integrating the magnetic energy density from inner radius R_i to outer radius R_e. It results in $W_m = 0.35 \, \mu$J.

The air-gap inductance is then computed as $L_{\sigma g} = 2 W_m/I^2 = 0.48 \, \mu$H. For the validation of the analytical model, a 2-D FE simulation of the straight-lined model at the inner radius R_i was carried out. The magnetic energy computed with the two methods is very close: The difference is lower than 1%. Hence, the total leakage inductance is $L = L_{\sigma,g} + L_{\sigma,\text{slot}} = 0.63 \, \mu$H.

Then, the FW capability can be computed. Referring to Fig. 6, it is possible to estimate the maximum speed (i.e., the speed where the power becomes zero). Adopting the normalized value, such a maximum speed is estimated as

$$\omega_{\max} = \frac{1}{\lambda_m - li} = 1.7 \text{ per unit.} \qquad (8)$$

Therefore, the AxF machine does not satisfy the required CPSR, and the phase inductance has to be increased. Imposing that the normalized PM flux linkage is equal to the required

value of 0.8 per unit, it is possible to compute the proper inductance so as to achieve the desired CPSR = 3. It is

$$L_{\text{tot}} = \frac{\Lambda_m}{I} \sqrt{\frac{1 - 0.8^2}{0.8^2}} = 1.2 \, \mu\text{H.} \qquad (9)$$

Hence, an additional leakage inductance should be added: $L_{\text{add}} = L_{\text{tot}} - L = 0.57 \, \mu$H. The necessary additional inductance is obtained by introducing C-shape double core into the end winding, as shown in Figs. 1 and 2. The actual geometry of the additional leakage inductance is shown in Fig. 7.

At the maximum current, the flux density in the core is computed to be $B = 1.22$ T. This is an acceptable value for the flux density in the iron core, avoiding additional core losses. The maximum normalized speed with the additional inductance becomes

$$\omega_{\max} = \frac{1}{\lambda_m - l_{\text{tot}} i} = 5.56 \text{ per unit.} \qquad (10)$$

The phasor diagram with additional inductance under nominal load is shown in Fig. 8.

At last, the actual number of conductors per slot is fixed according to the available voltage. The motor is supplied by a three-phase inverter with a dc bus $V_{\text{dc}} = 300$ V. Considering a voltage drop of 5%, the number of conductors per slot is estimated to be $n_c = 150$.

B. Further Advantages

The topology selected for the winding yields further advantages as the reduction of the cogging torque, of the Joule losses for a given torque, and of the short-circuit current [19]. The ratio between the short-circuit current and the nominal current can be estimated as $i_{\text{shc}}/i = \lambda_m/l_{\text{tot}} = 1.33$ per unit, i.e., the
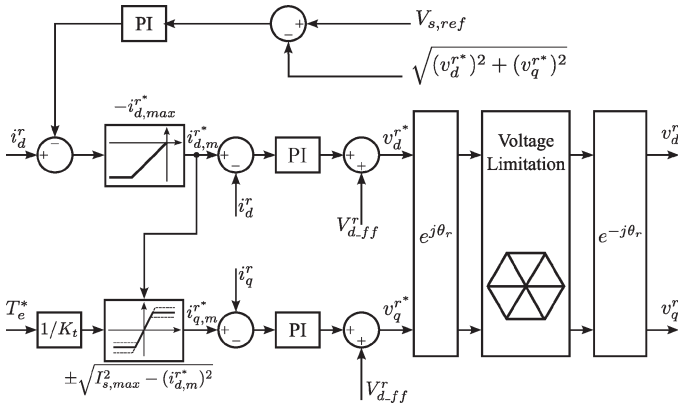
Fig. 9. Conventional FW method based on the voltage-magnitude feedback.
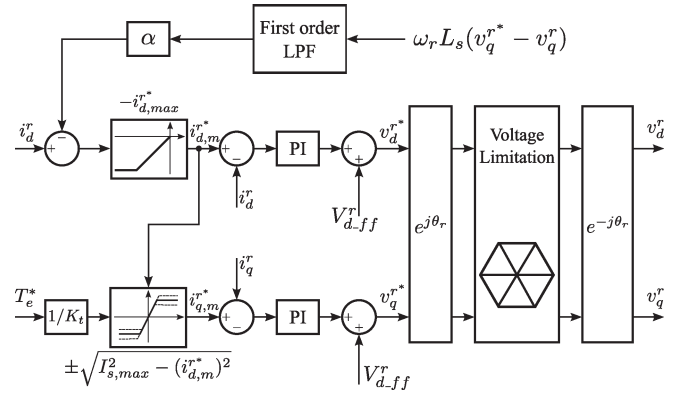

Fig. 11. FW method based on the voltage-difference feedback.
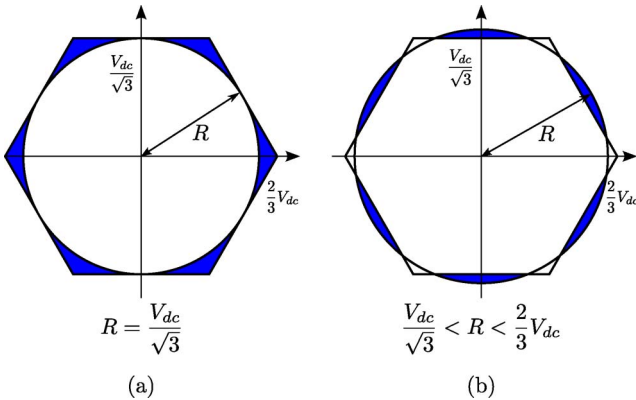

Fig. 10. Voltage-limit hexagon and voltage magnitude.

short-circuit current is only 33% higher than the nominal one. This ratio was also proved by experimental test.

In addition, in the 12-slot 10-pole configuration, there is no mutual coupling among the phases, with an increasing fault-tolerant capability. This winding topology is also characterized by the low back-EMF harmonic contents, as confirmed by experimental tests (reported in Section IV).

At last, the adopted solution with the external C-shape cores reluctances has the additional advantage of an easy adjustment of the value of the leakage inductance. In this way, the CPSR value can be adjusted according to different machine applications.

III. MACHINE CONTROL STRATEGY

The FW controller for the SPM motor has been widely researched, and in most of these researches, the magnitude of the voltage reference is fed back to regulate it to a certain value, as shown in Fig. 9 [10]–[12].

However, this control scheme cannot exploit the maximum available capacity of the drive system including the ac machine. To achieve that, it is important to get the maximum ac output voltage from given dc-link voltage of the inverter, while the FW controller shown in Fig. 9 fails to get the maximized ac voltage from the dc link.

As shown in Fig. 10, although the output voltage vector of a three-phase PWM inverter is limited by a hexagon, the conventional FW control limits the output voltage to a circle, whose radius is the voltage reference magnitude, as shown in Fig. 10(a).

If this magnitude is set to $V_{\rm dc}/\sqrt{3}$ as shown in Fig. 10(b), the shaded area of the voltage hexagon, i.e., the dc-link voltage, is not used. In other words, the capacity of the drive system is not completely utilized.

On the contrary, if the magnitude is set to a certain value larger than $V_{\rm dc}/\sqrt{3}$, as shown in Fig. 10(b), then the shaded area of the voltage reference circle would not be realized by the PWM inverter, and the current response may be degraded or, sometimes, the current controller may be unstable due to the windup phenomenon of the current-regulator integrator.

In order to assure the stable current control in the case shown in Fig. 10(b), an antiwindup strategy has to be incorporated with the current regulator, but the conventional antiwindup method shifts the current reference to a realizable one which cannot generate maximum available torque [13], [20].

Fig. 11 shows the block diagram of the control strategy in [13]. The difference between the q-axis reference voltage and the q-axis limited voltage modifies the d-axis current reference. As long as this difference is zero, the d-axis current reference will not be modified and equal to zero to satisfy the maximum torque per ampere condition.

The q-axis current reference should be limited in order that the magnitude of the current-reference vector does not exceed the current-magnitude limit. The modified current references can be expressed as

$$i_{d,m}^{r^*} = i_d^{r^*} - \frac{\alpha \omega_c}{s + \omega_c}(\omega_r L_s \Delta v_q^r)$$

$$i_{q,m}^{r^*} = \frac{i_q^{r^*}}{|i_q^{r^*}|} \min\left(|i_q^{r^*}|, \sqrt{I_{S,\max}^2 - |i_{d,m}^{r^*}|}\right) \quad (11)$$

where $\Delta v_q^r = v_q^{r^*} - v_q^r$ and α is a positive gain that affects the transient performance and the steady-state torque per ampere ratio [13].

Assuming that the synchronous PI current controller has an effective method to decouple the cross-coupled EMF terms [21], [22] and they are completely decoupled, the modified d-axis current reference can be expressed as

$$i_{d,m}^{r^*} = i_d^{r^*} - \frac{\alpha \omega_r L_s K_i}{K_p s + K_i} \Delta v_q^r$$

$$= i_d^{r^*} - \alpha \omega_r L_s \left(\frac{K_i}{s}\left(i_{q,m}^{r^*} - i_q^r\right) - R_s i_q^r\right). \quad (12)$$
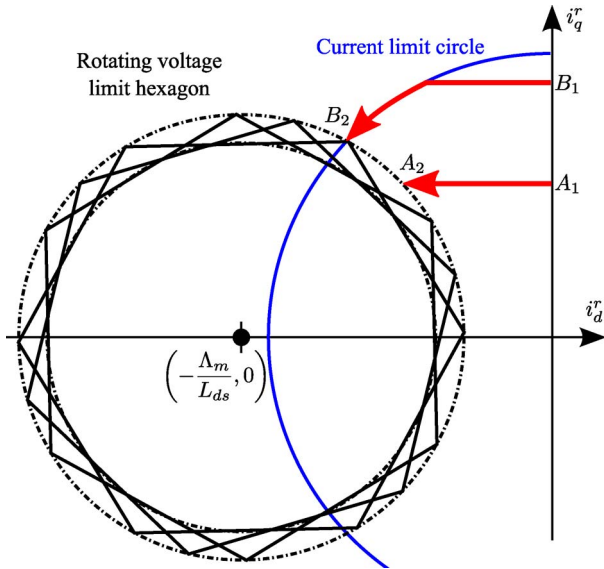
Fig. 12. Modified current-reference trajectory of the proposed method.

The cutoff frequency of the first-order low-pass filter is set to the corner frequency of the current controller K_i/K_p, where $K_i = R_s \omega_c$, $K_p = L_s \omega_c$, and ω_c, R_s, and L_s are, respectively, the bandwidth of current controller, the resistance of the stator, and the synchronous inductance.

From (12), it can be known that the modified d-axis current reference is affected by the integral term of the q-axis current controller and will be increased negatively until the q-axis current tracks the q-axis-modified reference. Thus, the proposed method can utilize the dc-link voltage better than the voltage-magnitude-feedback method in [10] and [11].

Even if the cross-coupled voltages cannot be canceled perfectly due to the variation of the machine parameters, the performance of this controller is not degraded severely because the integrators of the current controller internally compensate the cross-coupled voltage which is not decoupled perfectly.

Fig. 12 shows the migration of the operating point with this method in the synchronously rotating $d-q$ current plane. In Fig. 12, the voltage limit is represented by a rotating hexagon, because the voltage-limit hexagon in the stationary $d-q$ voltage plane can be considered as rotating backward at synchronous speed.

If the point A_1 is given for current references at a certain rotor speed beyond the motor base speed, then it moves toward the negative direction on the d-axis by (11) and reaches the point A_2. The point A_2 is out of the voltage-limit circle which radius is $V_{dc}\sqrt{3}$ or $2V_{dc}/\pi$, but it is on the rotating voltage-limit hexagon. Thus, the proposed method utilizes the dc-link voltage better than the other method based on voltage-magnitude feedback [10], [11].

For the case of point B_1, the current references are modified to the point B_2 by (11).

IV. EXPERIMENTAL RESULTS

The prototype has been tested on a test bench. Fig. 13 shows the experimental setup. The machine under test is loaded by an induction motor that can be operated in speed-control mode.
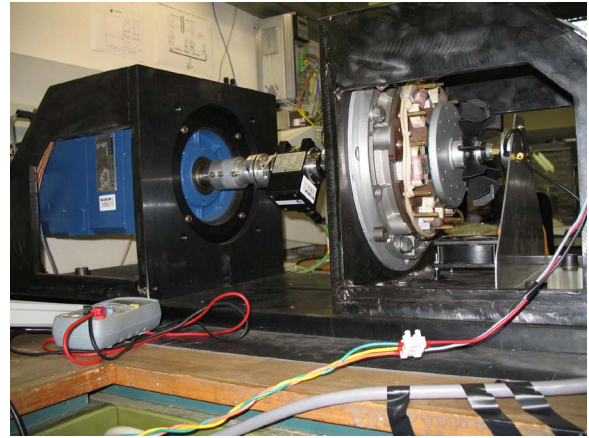

Fig. 13. Test bench for the measure.

TABLE III
PARAMETERS OF THE AxF PROTOTYPE

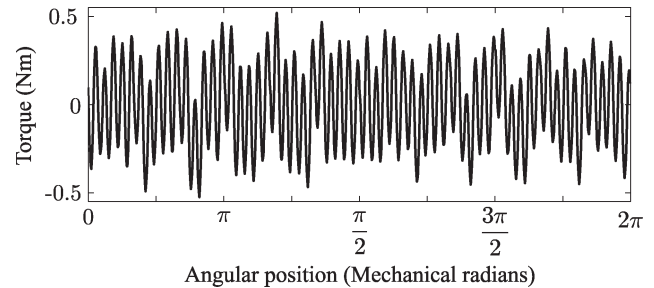|	Predicted	Measured
PM flux linkage (Vs)	0.220	0.197
Synchronous inductance (mH)	27.1	27.2
Stator resistance (Ω)	1.3	1.3

Fig. 14. Measured cogging torque of the AxF prototype.

The measures reported in this section have been carried out with a reduced voltage so as to fix the base speed to be equal to 500 r/min. This is due to some mechanical problems of the prototype, in order to retain the PMs in the rotor structure, against the centrifugal force. For safety sake, the tests were carried out at lower speed and, consequently, at lower voltage (proportionally reduced). Anyway, the effect of the inductance increase and the modified FW control algorithm on the CPSR wideness remains the same (of course, at lower power).

Table III reports a comparison between the predicted and the measured parameters of the machine. A reasonable agreement is found, except for the PM flux linkage. The difference between prediction and measurement is about 12%. This is due to the adoption of a simple analytical model to estimate the flux density and, probably, to a PM residual flux density B_{rem} lower than declared by the manufacturer.

Fig. 14 shows the measured cogging torque of the prototype. The motor is running at low speed, and the torque is measured by a torque meter. The peak-to-peak cogging torque is low, being less than 10% of the rated torque.

Fig. 15 shows the measured phase back EMF of the motor when the prototype run at 1000 r/min. As expected, due to the 12-slot 10-pole combination, the harmonic contents are limited.
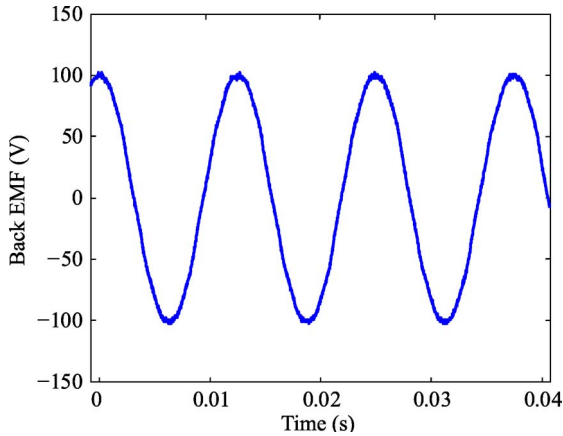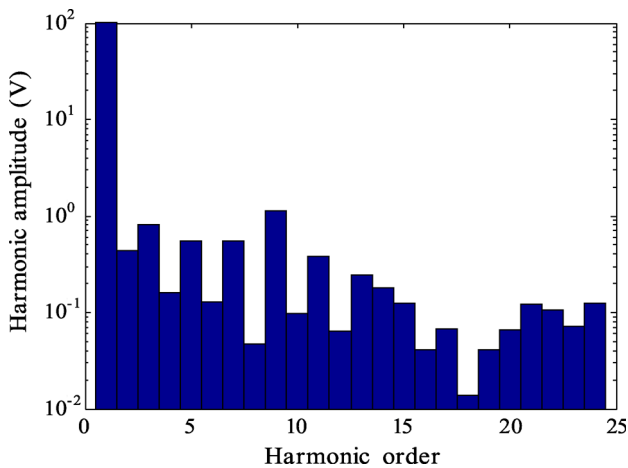
Fig. 15.   Measured back EMF of the AxF prototype.

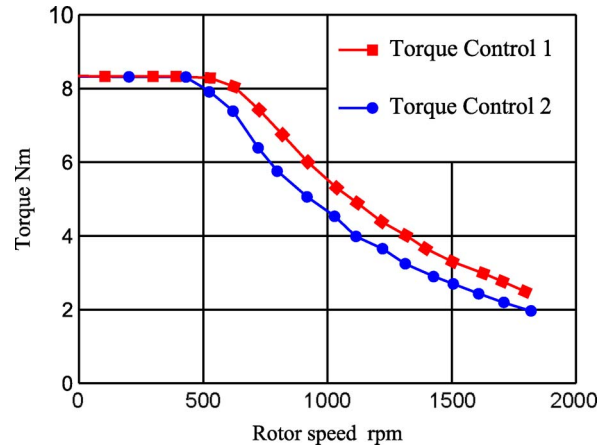Fig. 16.   Back EMF harmonic contents (fundamental harmonic is 103 V).

Fig. 17.   Torque characteristic of the AxF prototype (experimental tests). Two different control strategies are considered.
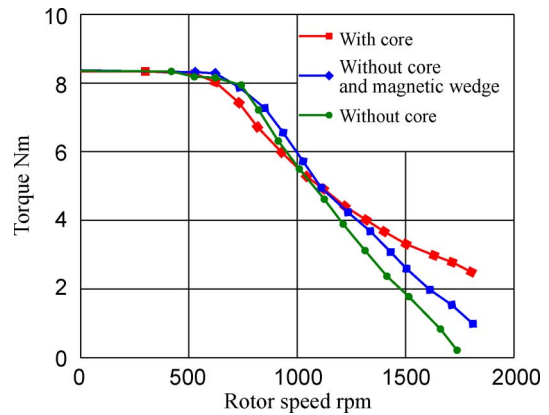

Fig. 18.   Torque-versus-speed curve of the three AxF prototypes (experimental tests with Torque Control 1).
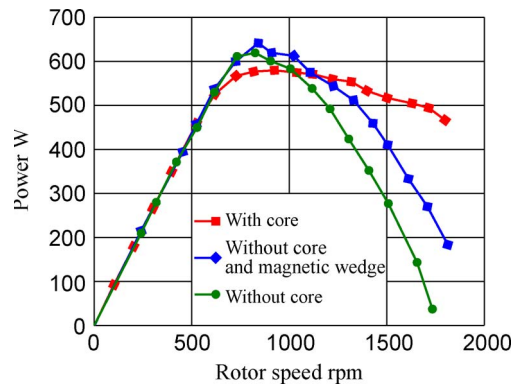

Fig. 19.   Power-versus-speed curve of the three AxF prototypes (experimental tests with Torque Control 1).

Such harmonic contents are shown in Fig. 16. The highest harmonics are those on the order of third and ninth, which do not yield any torque contribution.

The rotor losses of the prototype are not negligible, reaching about 60 W at a speed of 500 r/min and about 150 W at 1000 r/min. The analysis of the rotor losses due to both MMF harmonics and slot openings is reported in [23]. Magnetic wedges reduce slightly the rotor losses, particularly those due to the slot openings.

Fig. 17 shows the behavior of the measured torque versus rotor speed. Torque Control 1 means that the FW controller proposed in this paper (Fig. 11) is used, and Torque Control 2 means that the classical FW controller proposed in [10] and [11] (Fig. 9) is used. It is worth noticing that the control method described in this paper can produce a torque about 6% higher than the other one.

Figs. 18 and 19 shows the torque-versus-speed and power-versus-speed curves of the prototype for different machine configurations, respectively. All curves are achieved with the Torque Control 1. The torque curve with squared marks is the same as that shown in Fig. 17.

In order to verify the effectiveness of the additional cores, the line with circle marks shows the torque and power curve without the cores in the end winding. As expected, the developed torque decreases rapidly as the speed gets increased.

Finally, magnetic wedges have been introduced in the stator slot openings. The resulting torque-versus-speed and power-versus-speed curves are shown using diamonds marks. A moderate increase of the CPSR is observed. Such wedges are used for closing the slots of high-power induction motors. The material used for the magnetic wedges is fiberglass–iron magnetic wedge with relative permeability equal to 20. Due to their moderate permeability, it is reasonable that they affect slightly the torque-versus-speed characteristic, as confirmed by the experimental tests. They seem to be better than soft magnetic composite wedges in order to reduce rotor losses [23].

V. Conclusion

This paper described an AxF machine characterized by an FW capability and a control algorithm to increase the performance of this kind of machine during FW operations. For the purpose of achieving a wide constant-power speed region, the AxF machine has been designed with slotted stator and fractional-slot windings and additional cores enclosing end windings.

The solution presented allows an easy adjustment of the synchronous inductance to be carried out, so that a proper CPSR is achieved. On the contrary, the prototype has an increased outer diameter and non-negligible rotor losses. In order to reduce these losses, magnetic wedges can be adopted to smooth the anisotropy of the stator. At the same time, the motor exhibits low EMF harmonic contents and low cogging torque.

This paper presents the detailed design of the AxF machine characterized by a high FW capability. The AxF prototype has been designed for an 8 N · m and a 3 : 1 FW operating range. In order to exploit full capability of the machine, an FW controller has been designed and implemented. With this method, the output torque in the FW region is higher than that achieved by using a conventional FW method based on the voltage-magnitude feedback.

The achieved results show that the effect of the magnetic wedges on the increase of the CPSR is limited, also because of the moderate permeability of the material used. An effective increase of the CPSR is obtained by adopting the additional cores. In addition, adjusting the inductance of such cores, lower or wider CPSR can be achieved. The final motor prototype, controlled by the proposed torque-control algorithm, allows the prefixed specification of CPSR = 3 to be satisfied.

Acknowledgment

References

[1] R. L. Ficheux, F. Caricchi, F. Crescimbini, and O. Honorati, "Axial-flux permanent-magnet motor for direct-drive elevator systems without machine room," *IEEE Trans. Ind. Appl.*, vol. 37, no. 6, pp. 1693–1701, Nov./Dec. 2001.

[2] K. M. Rahman, N. R. Patel, T. G. Ward, J. M. Nagashima, F. Caricchi, and F. Crescimbini, "Application of direct-drive wheel motor for fuel cell electric and hybrid electric vehicle propulsion system," *IEEE Trans. Ind. Appl.*, vol. 42, no. 5, pp. 1185–1192, Sep./Oct. 2006.

[3] E. Muljadi, C. P. Butterfield, and Y.-H. Wan, "Axial-flux modular permanent-magnet generator with a toroidal winding for wind-turbine applications," *IEEE Trans. Ind. Appl.*, vol. 35, no. 4, pp. 831–836, Jul./Aug. 1999.

[4] F. Profumo, Z. Zhang, and A. Tenconi, "Axial flux machines drives: A new viable solution for electric cars," *IEEE Trans. Ind. Electron.*, vol. 44, no. 1, pp. 39–45, Feb. 1997.

[5] L. Del Ferraro, F. G. Capponi, R. Terrigi, and F. Caricchi, "Ironless axial flux PM machine with active mechanical flux weakening for automotive applications," in *Conf. Rec. 41st IEEE IAS Annu. Meeting*, Tampa, FL, Oct. 2006, vol. 1, pp. 1–7.

[6] A. Di Napoli, O. Honorati, E. Santini, and L. Solero, "The use of soft magnetic materials for improving flux weakening capabilities of axial flux PM machines," in *Conf. Rec. IEEE IAS Annu. Meeting*, Rome, Italy, Oct. 8–12, 2000, vol. 1, pp. 202–207.

[7] M. Aydin, S. Huang, and T. A. Lipo, "A new axial flux surface mounted permanent magnet machine capable of field control," in *Conf. Rec. 37th IEEE IAS Annu. Meeting*, Oct. 13–18, 2002, vol. 2, pp. 1250–1257.

[8] J. A. Tapia, D. Gonzalez, R. R. Wallace, and M. A. Valenzuela, "Increasing field weakening capability of an axial flux PM machine," in *Conf. Rec. 39th IEEE IAS Annu. Meeting*, Oct. 3–7, 2004, vol. 3, pp. 1427–1431.

[9] F. Profumo, A. Tenconi, Z. Zhang, and A. Cavagnino, "Novel axial flux interior PM synchronous motor realized with powdered soft magnetic materials," in *Conf. Rec. 33rd IEEE IAS Annu. Meeting*, St. Louis, MO, Oct. 12–15, 1998, vol. 1, pp. 152–158.

[10] D. S. Maric, S. Hiti, C. C. Stancu, J. M. Nagashima, and D. B. Rutledge, "Two flux weakening schemes for surface-mounted permanent-magnet synchronous drives. Design and transient response considerations," in *Proc. IEEE ISIE*, Bled, Slovenia, Jul. 1999, vol. 2, pp. 673–678.

[11] J.-H. Song, J.-M. Kim, and S.-K. Sul, "A new robust SPMSM control to parameter variations in flux weakening region," in *Proc. IEEE IECON*, Taipei, Taiwan, Aug. 1996, vol. 2, pp. 1193–1198.

[12] S. D. Sudhoff, K. A. Corzine, and H. J. Hegner, "A flux-weakening strategy for current-regulated surface-mounted permanent-magnet machine drives," *IEEE Trans. Energy Convers.*, vol. 10, no. 3, pp. 431–437, Sep. 1995.

[13] T. S. Kwon and S. K. Sul, "Novel antiwindup of a current regulator of a surface-mounted permanent-magnet motor for flux-weakening control," *IEEE Trans. Ind. Appl.*, vol. 42, no. 5, pp. 1293–1300, Sep./Oct. 2006.

[14] N. Bianchi, S. Bolognani, and M. Dai Pre, "Magnetic loading of fractional-slot three-phase PM motors with non-overlapped coils," in *Conf. Rec. 41st IEEE IAS Annu. Meeting*, Tampa, FL, Oct. 8–12, 2006, vol. 1, pp. 35–43.

[15] A. M. El-Refaie and T. M. Jahns, "Optimal flux weakening in surface PM machines using fractional-slot concentrated windings," *IEEE Trans. Ind. Appl.*, vol. 41, no. 3, pp. 790–800, May/Jun. 2005.

[16] N. Bianchi and S. Bolognani, "Unified approach to the analysis and design of an AC motor drive for flux-weakening operations," in *Conf. Rec. 33rd IEEE IAS Annu. Meeting*, St. Louis, MO, Oct. 12–15, 1998, vol. 1, pp. 95–102.

[17] N. Bianchi and S. Bolognani, "Parameters and volt–ampere ratings of synchronous motor drive for flux-weakening applications," *IEEE Trans. Power Electron.*, vol. 12, no. 5, pp. 895–903, Dec. 1997.

[18] M. Liwschitz-Garik and C. C. Whipple, "Electric Machinery," in *A–C Machines*, vol. II. New York: Van Nostrand, 1960.

[19] N. Bianchi, M. Dai Pré, L. Alberti, and E. Fornasiero, *Theory and Design of Fractional-Slot PM Machines*, IEEE IAS Tutorial Course notes, presented at the IEEE IAS Annu. Meeting, New Orleans, LA, Sep. 23, 2007, available from CLEUP, Padova, Italy (info@cleup.it).

[20] H. Yoo and S.-K. Sul, "Novel current control strategy for maximum tracking operation under saturated voltage condition," in *Conf. Rec. 40th IEEE IAS Annu. Meeting*, Oct. 2–6, 2005, vol. 4, pp. 2533–2539.

[21] T. M. Rowan and R. J. Kerkman, "A new synchronous current regulator and an analysis of current-regulated PWM inverters," *IEEE Trans. Ind. Appl.*, vol. IA-22, no. 4, pp. 678–690, Jul./Aug. 1986.

[22] F. Briz, M. W. Degner, and R. D. Lorenz, "Analysis and design of current regulators using complex vectors," *IEEE Trans. Ind. Appl.*, vol. 36, no. 3, pp. 817–825, May/Jun. 2000.

[23] L. Alberti, E. Fornasiero, N. Bianchi, and S. Bolognani, "Impact of rotor losses in a 12-slot 10-pole axial flux PM machine," in *Conf. Rec. 43rd IEEE IAS Annu. Meeting*, Edmonton, AB, Canada, Oct. 5–9, 2008, [CD-ROM].

Tae-Suk Kwon (S'04–M'08) was born in Seoul, Korea, in 1973. He received the B.S. degree and the M.S. degree in electrical engineering from Hanyang University, Seoul, in 1995 and 1997, respectively, and the Ph.D. degree in electrical engineering from Seoul National University, Seoul, in 2007, where he is currently working toward a Postdoctoral degree in the School of Electrical Engineering and Computer Science.

From 1997 to 2003, he was a Research Engineer with the Technical R&D Center, Hyundai Elevator Company, Ltd., Ichon, Korea, where he developed high-speed gearless elevator systems. His interests include high-performance ac drive systems and hybrid electric vehicle drives.

Seung-Ki Sul (S'83–M'86–SM'98–F'00) was born in Korea in 1958. He received the B.S., M.S., and Ph.D. degrees in electrical engineering from Seoul National University, Seoul, Korea, in 1980, 1983, and 1986, respectively.

From 1986 to 1988, he was an Associate Researcher with the Department of Electrical and Computer Engineering, University of Wisconsin, Madison. From 1988 to 1990, he was a Principal Research Engineer with LG Industrial Systems Company. Since 1991, he has been a Faculty Member of the School of Electrical Engineering and Computer Science, Seoul National University, where he is currently a Professor. His current research interests include control of electric machines using power electronics, electric/hybrid vehicle drives, and power converter circuits.

Nicola Bianchi (M'98) was born in Verona in 1967. He received the M.S. and Ph.D. degrees in electrical engineering from the University of Padova, Padova, Italy, in 1991 and 1995, respectively.

Since 1998, he has been an Assistant Professor in the Electric Drives Laboratory, Department of Electrical Engineering, University of Padova. His research activity is in the field of design of electrical motors for electric drive applications. He is the coauthor of several papers on the subject of electrical machines and drives and the author of the international text *Electrical Machine Analysis Using Finite Elements* (CRC Press and Taylor & Francis Group, 2005) and two Italian textbooks.

Luigi Alberti (S'07) received the Laurea and Ph.D. degrees in electrical engineering from the University of Padova, Padova, Italy, in 2005 and 2009, respectively.

His research activities are concentrated on the electromechanical analysis and design of electrical motors, particularly for electric drive applications. He is also a Consultant to various electromechanical industries.